




Science-rich Sites for In Situ Resource Utilization Characterization and End-to-end Demonstration Missions

Carolyn H. van der Bogert¹ , Harald Hiesinger¹, Isacco Pretto², Floriano Venditti², Alexander Lewang¹, Lutz Richter³, David Binns⁴, and Philipp Gläser⁵

¹ Institut für Planetologie, Westfälische Wilhelms-Universität Münster, Wilhelm-Klemm-Str. 10, D-48149 Münster, Germany; vanderbogert@uni-muenster.de

² OHB Italia S.p.A., Via Gallarate 150, I-20151 Milan, Italy

³ OHB System AG, Manfred-Fuchs-Str. 1, D-82234 Weßling-Oberpaffenhofen, Germany

⁴ European Space Agency, European Space Research and Technology Centre, Keplerlaan 1, 2201 AZ Noordwijk, The Netherlands

⁵ Institut für Geodäsie und Geoinformationstechnik, Technische Universität Berlin, Straße des 17. Juni 135, D-10623 Berlin, Germany

Received 2020 November 1; revised 2021 March 7; accepted 2021 March 9; published 2021 April 30

Abstract

Within the European Space Agency’s “Commercial In Situ Resource Utilization (ISRU) Demonstration Mission Preparation Phase,” we examined two types of lunar sites in preparation for an ISRU demonstration mission. First, we considered poorly characterized potential resource sites. For these so-called characterization sites, precursor missions would investigate the material properties and address strategic knowledge gaps for their use as ISRU feedstock. Regions of interest for characterization missions include the Aristarchus plateau, Montes Harbinger/Rimae Prinz, Sulpicius Gallus, and Rima Bode. Regional pyroclastic deposits at the Aristarchus plateau and adjacent Montes Harbinger/Rimae Prinz exhibit remotely sensed low-Ti, high-Fe²⁺ compositions. They differ from the high-Ti pyroclastics at Rima Bode and Sulpicius Gallus, which are similar to the pyroclastics northwest of the Taurus Littrow valley (Apollo 17 site). Thus, exploration of the Aristarchus plateau would allow investigation of previously uncharacterized materials, whereas Rima Bode or Sulpicius Gallus would allow comparison to Apollo 17 pyroclastics. Any of these sites would enable evaluation of reported H₂O/OH in these deposits. Second, we examined a possible site for a direct ISRU demonstrator mission. For a stand-alone end-to-end (E2E) ISRU demonstrator, a fuller understanding of the physical and compositional characteristics of potential feedstock is required for mission risk reduction. In this case, locations near preexisting sites would allow extrapolation of ground truth to nearby deposits. Because a Ti-rich pyroclastic deposit appears advantageous from beneficiation and compositional perspectives, we examine an example E2E demo site northwest of the Taurus Littrow valley. Hydrogen and methane reduction, as well as the Fray–Farthing–Chen Cambridge process, could be tested there.

Unified Astronomy Thesaurus concepts: [Lunar science \(972\)](#); [Lunar surface \(974\)](#)

1. Introduction: Space Resources Strategies and Knowledge Gaps

Various methods for extracting oxygen, other volatiles, and metals from lunar regolith and pyroclastic deposits have been investigated for more than 50 yr (e.g., Mendell 1985; Taylor & Carrier 1992, 1993; Allen et al. 1996; Taylor & Martel 2003; Schunk et al. 2008; Anand et al. 2012; Schwandt et al. 2012; Crawford 2015; Lomax et al. 2020; Reiss et al. 2020; Sargent et al. 2020; Schlüter & Cowley 2020). Use of resources on the Moon is strategically important for longer-term lunar scientific and technological endeavors (e.g., Sanders & Larson 2015; European Space Agency 2019a; Bennett et al. 2020; Meurisse & Carpenter 2020; National Aeronautics and Space Administration 2020). Thus, space agencies have organized and supported technology development programs to advance in situ resource utilization (ISRU) technologies, which are motivated by filling strategic knowledge gaps (SKGs).

NASA developed a list of SKGs that are used to guide their robotic and human exploration strategies (National Aeronautics and Space Administration 2016). This list includes a section about lunar resource potential and has been reviewed and updated by the Lunar Exploration Analysis Group (LEAG; LEAG 2016). Several

of the SKGs remained open after the LEAG review: (1) continued characterization of Apollo regolith samples, (2) in situ characterization of lunar volatiles, (3) preservation of volatiles during mission operations, (4) geotechnical characterization of cold traps, (5) determinations of accessibility conditions at cold traps, (6) understand the charging and plasma environment in permanently shadowed regions, (7) examination of the nature of polar volatiles, (8) definition of volatile transport mechanisms and time frames, (9) characterization of pyroclastic deposits as resources, (10) definition of the efficiency of ISRU processes using regolith simulants, and (11) testing of ISRU processes on the Moon.

The European Space Agency (ESA)’s recently defined Space Resources Strategy (European Space Agency 2019a) focuses on industry and agency objectives for the next decade, which include (1) establishing whether and which resources can enable sustainable exploration (see also Carpenter et al. 2016), (2) enabling scientific and economic opportunities in Europe, (3) driving innovations for space and Earth applications, (4) encouraging new industry participation, and (5) cementing ESA’s international partner role. Activities related to these objectives reflect and expand on the NASA SKGs for lunar resources. In particular, by 2030, ESA aims to establish the volatiles resource potential of at least one nonpolar and one polar deposit, mature and demonstrate oxygen and other consumables production methods, test these on the lunar surface, and integrate the knowledge gained into the international exploration architecture (European Space Agency 2019a). In concert with technology development, specific



Original content from this work may be used under the terms of the [Creative Commons Attribution 4.0 licence](#). Any further distribution of this work must maintain attribution to the author(s) and the title of the work, journal citation and DOI.

related science goals are discussed in ESA's Strategy for Science at the Moon (European Space Agency 2019b). Within the next decade, it is planned to return lunar samples from at least two unexplored sites and analyze these in European laboratories; perform in situ measurements of polar volatiles (e.g., PROSPECT); deploy at least one geophysical package and retroreflector; characterize the compositional, mineralogical, and geophysical properties of a nonpolar resource deposit; make in situ measurements of the dust and plasma environment; and test the biological effects of the lunar environment (European Space Agency 2019b; see also Carpenter et al. 2012).

Within this framework, ESA's Commercial ISRU Demonstration Mission Preparation Phase study sought to address and prepare to address ISRU SKGs by driving development of industrial ISRU technologies (1) via design and implementation of ISRU processing of lunar simulants in terrestrial laboratories and (2) as a payload for an ISRU technology demonstrator on the lunar surface. The study included definitions and development for three mission types: (1) a technology demonstration for critical enabling technologies, (2) a characterization mission including assessment of the compositional and physical properties of potential ISRU feedstock, and (3) a small-scale ISRU demonstration plant (Binns et al. 2018; Meurisse & Carpenter 2019; Pretto et al. 2020). As part of the study, the potential roles and contributions of commercial lander services were also evaluated. It is within this context that we performed a study for one of the industry partners to identify both technologically relevant and scientifically rich landing sites for the latter two mission types.

2. Study Approach

First, we define the engineering framework for the preparation of ESA's commercial in situ demonstration missions, because this has a significant effect on the selection of suitable landing sites. Then, we review the lunar sites discussed in the peer-reviewed literature (e.g., Flahaut et al. 2012; Kring & Durda 2012; Keller et al. 2016; Jawin et al. 2019) for various science and/or technology missions and assess their relevance as either ISRU characterization or end-to-end (E2E) demonstrator sites. This overview is not based on a new detailed global assessment of various data sets; rather, it relies on the state of knowledge as presented in the literature. Next, we define a set of site selection criteria based on the engineering constraints to filter the possible landing sites down to a refined list of ISRU-relevant sites. From this list, we examine and discuss sites that need additional characterization of compositional, mineralogical, and physical properties to address SKGs for ISRU applications. Finally, we provide an example landing site for a direct E2E demonstrator, based on knowledge gained from the Apollo program.

3. Engineering Considerations and Constraints

The engineering constraints on the selection of ISRU study sites are multifaceted. First, the delivery system—here a commercial service—has constraints for entry, descent, and landing, including hazard avoidance capabilities. Additional constraints arise from the payloads themselves, whether it is a characterization or E2E demonstrator payload.

3.1. Landing Systems

Alongside our study, ESA examined the feasibility of using commercial landing services for delivering the payloads to the

Moon and provided us with their constraints for latitude ranges and landing ellipse dimensions. The two participating providers specified a combined reachable latitude range of 0° – 45° N/S. The definition of the landing ellipse dimensions was refined as the study proceeded, with a relatively large tens of kilometers major axis reducing to slightly less than 1 km by the end of the study. This dynamic requirement initially drove us to select regions with extensive deposits of interest. We also excluded regions of interest (ROIs) on the farside of the Moon because this would require a communications satellite, thus increasing the cost and complexity of a mission.

Landers will also need to avoid boulders and craters at the landing sites. A preliminary view of the potential danger posed by boulders and fresh craters is made via the Lunar Reconnaissance Orbiter (LRO) Diviner rock abundance map (Bandfield et al. 2011) and LRO Narrow Angle Camera (NAC) digital terrain models (DTMs). Further higher-resolution analyses, including generation of terrain roughness indices (TRIs), can be performed to directly measure the size frequencies of craters and boulders within the selected study areas to provide a fuller view of the size and areal distribution of these hazards. Imaging at high illumination angles (low Sun) can also aid in identification of small boulders and craters from long cast shadows.

Due to the constraint of landing opportunities to the mid-latitudes, potential sites discussed in this report receive approximately 14 days of illumination per lunar day. The illumination conditions and surface temperature changes through the lunar day can be calculated using a combination of topographic models and brightness temperature data and calibrated to Apollo heat flow measurements (e.g., Bauch et al. 2014; Williams et al. 2017; Gläser et al. 2018; Gläser & Gläser 2019). At the time of the study, requirements for solar insolation (power supply) or temperature limits for the landers were not provided. However, the work here can be augmented once such requirements are available.

3.2. Characterization Payload

The characterization payload is designed to collect information about the compositional, mineralogical, and physical characteristics of potential feedstock materials that have previously not been well characterized. The landed package would include a suite of instruments, including a context camera, visible/infrared spectrometer, laser-induced breakdown spectrometer (LIBS), and volatiles sampler, housed on a small rover to allow analysis of materials away from the lander and the effects of thruster operation.

The visible/infrared spectrometer would build on the MicrOmega-IR instrument developed by a European/Russian consortium for the ExoMars 2022 rover (e.g., Bibring et al. 2017). LIBS instrumentation for the detection of volatiles is being developed by industry and the German Space Agency (Vogt et al. 2020) for inclusion on a lunar volatiles sampler (LVS) package called Lunar Volatiles Mobile Instrumentation Extended (LUVMI-X) that is also supported by EU funding (Biswas et al. 2020). The LVS is a drill-like instrument tailored to lunar surface missions that places an electric heater into the lunar regolith to a shallow depth of down to ~ 20 cm. Through in-place heating, embedded volatiles are gasified and then analyzed by a miniature ion trap mass spectrometer. The E2E demonstrators of the LVS have been developed and tested in simulated lunar conditions, thus reaching a technical readiness

level of 5. Currently, the LVS is going through a formal preliminary design review (PDR) process with ESA, with the expectation that it could be ready for flight by late 2023. Geotechnical characteristics of the regolith can be examined, for example, using the robotic arm motor currents during excavation and/or the volatiles sampler drill telemetry, as well as context imaging of undisturbed and disturbed surfaces.

The characterization payload in particular aims to address SKGs regarding lunar resources: (1) assess the amounts, distribution, and forms of hydrogen species and other volatiles in regolith and (2) evaluate the compositions, distributions, and forms of pyroclastic deposits and their associated volatiles (e.g., LEAG 2016). These data would not only address technical SKGs, but also contribute to fundamental science (e.g., Jawin et al. 2019).

3.3. E2E Demonstrator Payload

To select a landing site for an E2E demonstrator, the compositional and physical properties of the feedstock need to be well established. Thus, an E2E mission would need to follow a characterization mission or land in the vicinity of prior missions, where the materials have been well characterized. Many detailed studies of lunar soil characteristics stemmed from Apollo and Luna sample studies (e.g., Carrier 1973, 1974, 2003, 2005; Carrier et al. 1991; Lindsay 1976; Simon et al. 1981; Morris et al. 1983; McKay et al. 1991; Graf 1993; Cooper 2007).

Different oxygen extraction methods were explored by industry during the ESA project to achieve the primary goal of driving the development of ISRU technologies. In particular, three methods have been recently examined in the scope of this and other ESA activities: hydrogen reduction, carbothermal or methane reduction, and the Fray–Farthing–Chen (FFC) Cambridge (electrodeoxidation) processes (e.g., Lomax et al. 2020; Reiss et al. 2020; Sargent et al. 2020; Schlüter & Cowley 2020). Each method imposes different requirements on the feedstock. For example, ilmenite reduction using hydrogen or methane is one of the most extensively studied mechanisms to extract oxygen (e.g., Taylor & Carrier 1992; Schwandt et al. 2012). However, the basalts containing the highest Ti levels (up to ~20% ilmenite) are found in two rather limited geographic regions: western Oceanus Procellarum and eastern Mare Tranquillitatis (e.g., Crawford 2015). Indeed, the reduction of volcanic glasses (up to ~16 wt% TiO₂; Delano 1986) is likely more advantageous due to their greater abundance and extent, in addition to the greater ease with which they can be prepared for ISRU processing (e.g., Mendell 1985; Hawke et al. 1990; Table 1). Other methods under development would also be applicable to the processing of silicate-rich materials, including those with few to no Fe/Ti minerals: carbothermal/methane reduction (Cutler & Krag 1985; Rice et al. 1997; Preto et al. 2020) and the electrochemical FFC Cambridge process (Schwandt et al. 2012; Lomax et al. 2020).

For the first E2E mission, it is not foreseen that complex beneficiation steps would be used. Thus, the demo feedstock must have a narrow range of grain sizes and be easily scooped into the demo plant with minimal processing. Thus, pyroclastic soils—comprising mostly volcanic glass with typical grain sizes of 40–100 μm—would be ideal starter feedstock (e.g., Hawke et al. 1990; Taylor & Carrier 1992; Lawrence & Hawke 2008).

An E2E ISRU demonstration will be most effectively achieved on a surface with low slopes. Therefore, locations

Table 1
Pyroclastic Deposits with Extents Exceeding 2500 km²

Location	Latitude	Longitude	Area (km ²)	Enhanced H ₂ O/OH
Aristarchus	26.7	−50.5	37,400	*
Taurus Littrow	20.1	30.1	4000	*
Sulpicius Gallus	20	10	6000	*
Montes Harbinger	20	−42	5400	*
Montes Carpatus	15	−25	2500	
Rima Bode	13	−3	10,000	*
Mare Vaporum	10	7	10,000	*
Sinus Aestuum	5	−7	30,000	*
Mare Humorum	−30	−40	3000	*

Note. List modified from the USGS Pyroclastic Volcanism Project database (<https://astrogeology.usgs.gov/geology/moon-pyroclastic-volcanism-project>) and sorted by latitude. Occurrences marked with a star exhibit indigenous water or OH (Milliken & Li 2017).

that have slopes of >5° in DTMs will be excluded from the possible ROIs.

4. Previously Proposed Sites of Interest for ISRU

Previously proposed sites for nonpolar oxygen extraction ISRU often focus on the investigation of pyroclastic deposits and high-TiO₂ basalt units. Extensive regional dark mantling deposits (RDMDs; e.g., Table 1) have been of interest for ISRU potential for decades and were proposed as sites for a lunar base prior to the discovery of polar volatiles (e.g., Mendell 1985; Hawke et al. 1990; Lawrence & Hawke 2008). The RDMDs can be separated into two different spectral types: (1) possibly Fe²⁺-bearing volcanic glasses that exhibit broad, long-wavelength absorption features (e.g., the Aristarchus plateau, the largest RDMD) and (2) ilmenite-bearing pyroclastics (e.g., Gaddis et al. 1985; Lucey et al. 1986). The latter were sampled at the Apollo 17 landing site in Taurus Littrow, although it is unknown how representative these materials are of other RDMDs (Lawrence & Hawke 2008). These TiO₂-rich, ilmenite-bearing materials have been the focus of numerous studies of oxygen extraction, particularly via hydrogen reduction of the ilmenite (e.g., Hawke et al. 1990; Taylor & Carrier 1992; Allen et al. 1996).

Pyroclastic deposits are described as particularly advantageous for ISRU testing and development because (1) they are fine-grained, well sorted, and generally boulder-free, and (2) they have a narrow average grain size of ~40–100 μm (based on Apollo studies; Taylor & Carrier 1992; Lawrence & Hawke 2008). These characteristics may allow for easy excavation and handling, whereas basalt deposits would require more beneficiation due to the presence of boulders or intact flow units. In addition to being a feedstock for oxygen extraction, pyroclastics may also contain solar wind implanted and/or endogenous volatiles (e.g., Milliken & Li 2017; Kornuta et al. 2018).

In the following sections, we review existing ROIs and proposed landing sites encompassing both pyroclastic and basaltic deposits and compile a list of locations we then evaluate for either characterization or E2E ISRU demonstrator missions.

4.1. Heritage from NASA's Constellation Program

One of the goals for NASA's LRO mission was to collect high-resolution data for ROIs for NASA's now-defunct

Constellation program (Gruener 2009; Vondrak et al. 2010; Keller et al. 2016). The ROIs (http://wms.lroc.asu.edu/lroc/view_rdr/SHAPEFILE_CX_TARGETS) address various scientific goals defined in the 2007 National Research Council (NRC) Scientific Context for the Exploration of the Moon (NRC 2007) report and have complete high-resolution data coverage, including photometric and geometric stereo imaging (Keller et al. 2016). For oxygen extraction, particularly hydrogen or methane reduction methods, Constellation ROIs for ISRU feedstock investigations and technology demonstrations include pyroclastic deposits (Aristarchus, Sulpicius Gallus, Rima Bode, Alphonsus Crater, Schrödinger basin) or iron- and/or titanium-rich mare deposits and their regolith (the Flamsteed crater, Mare Tranquillitatis, Mare Smythii, Mare Moscoviense).

4.2. Lunar Science for Landed Missions Workshop

A recent workshop cosponsored by NASA's Solar System Exploration Research Virtual Institute and LEAG compiled proposed sites for landed science from the scientific community (Jawin et al. 2019). The sites were evaluated on the basis of their ability to address scientific goals defined by three reports: (1) the 2007 NRC report (NRC 2007), (2) the LEAG report "Advancing Science of the Moon" (LEAG 2017), and (3) the NRC's Planetary Decadal Survey for 2013–2022 (NRC 2011). Several ROIs that may be relevant for oxygen extraction were proposed by the workshop participants: Aristarchus, the Compton–Belkovich volcanic deposit, the Gruithuisen domes, Marius Hills, Moscoviense, Orientale, the P60 mare basalt unit, Rima Bode, and Schrödinger basin. These ROIs were selected based on their relevance to science themes, but some of them also provide an opportunity for ground-truthing materials useful for resource extraction. Thus, these locations also address SKGs that relate to the understanding of their lunar resource potential (National Aeronautics and Space Administration 2016).

4.3. Global Landing Site Studies for Maximizing Science Return

Kring & Durda (2012) summarized seven science concepts drawn from the NRC (2007) report and compiled the work of a 5 yr period of Lunar and Planetary Institute summer studies interns to provide a global assessment of landing sites that address multiple science concepts. In the context of the characterization of ISRU sites, high-Ti mare basalts (types M1 and M2, as spectrally defined by Chevrel et al. 2002), primarily located within Mare Tranquillitatis and eastern Oceanus Procellarum, as well as pyroclastic deposits, are of particular relevance. In the study, they identified locations that allow sampling of a variety of high-Ti mare deposits, floor-fractured crater materials, and pyroclastics, for example, in Oppenheimer, Grimaldi, Mare Smythii, and Mare Moscoviense. In general, these landing site recommendations require mobility for access to the diverse materials.

Flahaut et al. (2012) used the NRC (2007) report to support a global study of science-rich landing sites for lander missions using integrated remote-sensing data sets. Their work focused on NRC (2007) themes dealing with the lithological diversity of the lunar surface. As such, they assessed mare basalt and pyroclastic deposit locations. The basalt types of Chevrel et al. (2002) include M1 and M2 basalts with high titanium contents and M3 and M4 basalts with moderate titanium contents, with all having differing thorium contents. The M5 type represents

basalt with low titanium and iron contents. Flahaut et al. (2012) pointed out that the M1, M3, and M4 basalt types have been sampled by the Apollo and Luna missions, while the M2 and M5 types have not been sampled. Specific recommendations for landing sites addressing these basalt types were not explicitly presented in the publication. However, they ranked sites by their ability to meet a range of NRC (2007) scientific goals; those that also exhibit pyroclastic or basaltic deposits are Aristarchus (ranked No. 4), Humorum (No. 8), Nectaris (No. 13), Smythii (No. 14), Balmer-Kapteyn (No. 15), Grimaldi (No. 17), Marginis (No. 19), and Alphonsus (No. 27).

Both of these global studies and related publications examined the scientific goals for understanding the Moon and selected areas where as many of these goals as possible could be addressed within a small area. While a geologically complex landing site with access to many different materials is advantageous for a rover or human mission, an ISRU characterization site should have a simple geology to foster a straightforward understanding of the potential resource materials. As a result, we did not evaluate these rich but more complicated sites in the scope of an ISRU characterization mission. However, the regions and rock types discussed above provide some additional perspectives on important science questions that may be addressed during an ISRU-related mission.

5. Site Selection Strategy

We down-select possible sites based on (1) engineering constraints provided by two potential commercial lander providers, (2) exclusion of areas that are neither pyroclastic nor basaltic due to current beneficiation constraints and the desire to test different ISRU methods, (3) deselection of locations that have limited areal extent, and (4) a ranking of the sites based on remotely sensed indigenous OH/H₂O content. Finally, we review which locations are covered by LRO NAC stereo and/or controlled mosaic observations. Stereo observations are important for the generation of high-resolution DTMs, and while they can be requested from the LRO Camera (LROC) team, limited opportunities are available for such observations. Considerations of areal extent reflect both technical and scientific factors; (a) a larger area gives a larger region in which to select landing sites optimized for the engineering requirements, and (b) examination of local and/or unique materials is less likely to provide ground truth that can be extended to other parts of the Moon. A consideration of locations with high concentrations of indigenous water seeks to augment the goals of an ISRU characterization mission for oxygen extraction feedstock to collect additional information about potentially useful hydrogen.

6. Potential ISRU Characterization Sites

The characterization site ROIs generally fall into four groups (Table 2): (1) high-TiO₂ pyroclastics with affinity to the Apollo 17 site, (2) high-FeO, low-TiO₂ pyroclastics characterized by the Aristarchus plateau materials, (3) high-TiO₂ basalt (e.g., type M2), and (4) high-FeO, lower-TiO₂ basalts (e.g., the P60 basalt; Hiesinger et al. 2003). The group 1 regions include Sinus Aestuum, Rima Bode, Mare Vaporum, and Sulpicius Gallus. High-TiO₂ pyroclastics were sampled at the Apollo 17 landing site, but it is unknown how these deposits compare to the others that have only been observed via remote sensing (Lawrence & Hawke 2008). Group 2 is primarily represented

Table 2
Potential ISRU Characterization and Demo Sites

Group	Location	Lat.	Long.	Description
(1) High-TiO ₂ pyroclastics	Taurus Littrow valley	20.2	30.8	Regional high TiO₂
	Sulpicius Gallus	19.87	10.37	Regional high TiO₂, H₂O/OH
	Rima Bode	12.9	-3.8	Regional high TiO₂, H₂O/OH
	Sinus Aestuum	5	-7	Regional high TiO ₂
	Mare Vaporum	10	7	Regional high TiO ₂ , H ₂ O/OH
(2) High-Fe/low-TiO ₂ pyroclastics	Aristarchus	27.7	-52.4	Regional Fe²⁺, H₂O/OH
	M. Harbinger/R. Prinz	20	-42	Regional Fe²⁺, H₂O/OH
	M. Humor/Doppelmayer	-30	-40	Regional, H ₂ O/OH
(3) High-TiO ₂ basalts	Mare Tranquillitatis	6.93	22.06	High TiO ₂ <12.6 wt% TiO ₂
	Lichtenberg crater	31.65	-67.23	High-TiO ₂ basalt nearby
	Flamsteed crater	-2.45	-43.22	High-TiO ₂ basalt nearby
	Marius Hills	13.58	-55.8	Volcanic province
(4) High-FeO basalts	P60 basalt	22.5	-53.8	Young, low-TiO ₂ basalt
	Mare Crisium	10.68	58.84	Low TiO ₂ <8.1 wt% TiO ₂

Note. Nearside ROIs meeting the engineering constraints. Higher-priority sites are marked in bold (see Section 6). Coordinates are approximate given the need for additional detailed hazard evaluation.

by the low-TiO₂ and high-Fe²⁺ compositions of the largest lunar pyroclastic on the Aristarchus plateau. Within group 3, the high-TiO₂ basalts of type M2 are not present in our sample collection (Flahaut et al. 2012). A final, fourth group includes lower-TiO₂, high-FeO basalts such as the P60 basalt (Hiesinger et al. 2003; Stadermann et al. 2018; Jawin et al. 2019), which is one of the youngest basalts on the Moon.

The first two groups exhibit potentially high concentrations of indigenous H₂O/OH as observed by Milliken & Li (2017). Given the need for the ground truth of these values and the potential use of indigenous water as an ISRU resource, it may be beneficial to select a landing site that also exhibits high indigenous water contents. These locations are, for group 1, Sulpicius Gallus, Rima Bode, or Humor/Doppelmayer, and, for group 2, the Aristarchus plateau. In the next sections, we discuss these groups in more detail.

6.1. High-TiO₂ Pyroclastics (Group 1)

Rima Bode is a ca. 10,000 km² regional pyroclastic deposit with high (>10 wt%) TiO₂ contents that is northeast of a larger regional pyroclastic deposit in Sinus Aestuum (Figure 1(a)). The spectral characteristics of both deposits are similar to those of the pyroclastic deposits to the northwest of the Apollo 17 landing site. Figure 1(b) shows the area in the Clementine color ratio map that is composed of the following band ratios: red = 750/415 nm, green = 750/950 nm, and blue 414/750 nm (McEwen et al. 1994; Pieters et al. 1994). The map emphasizes the range of soil compositions and maturities while minimizing the effect of albedo and topography. Thus, iron-rich basaltic materials (maria) with low titanium contents are shown in yellow/orange colors, while maria with higher titanium contents appear blue, and pyroclastic deposits with high iron and titanium contents look purple (McEwen et al. 1994; Pieters et al. 1994). While Sinus Aestuum, also with TiO₂ contents >10 wt%, is larger in extent than Rima Bode, it exhibits no reported H₂O/OH content compared with Rima Bode, where values are ≥300 ppm (Milliken & Li 2017). As a result, we give Rima Bode a higher ranking than Sinus Aestuum in terms of priority (Table 2).

Rima Bode exhibits a thick, central deposit with patchy, thinner deposits at its margins (Gaddis et al. 2003; Jawin et al. 2019). Characterization of Rima Bode materials could contribute to the

scientific understanding of the volatile budget and volcanic evolution on the Moon. Key measurements recommended by Jawin et al. (2019) include chemistry and mineralogy, volatile contents, and geomechanical regolith properties. LRO NAC stereo observations, DTMs, and controlled mosaics exist for locations both at Rima Bode and in southeast Sinus Aestuum (Figure 1(c)).

Sulpicius Gallus is a 6000 km² pyroclastic deposit with high (>8 wt%) TiO₂ contents (Figure 2(a)) about 500 km to the northeast of Rima Bode. The overall TiO₂ values are slightly lower, and the deposits are somewhat patchier, than at Rima Bode. However, the areal extent of the indigenous water signature (≥300 ppm) is somewhat larger at Sulpicius Gallus. Also shown in Figure 2 is the 10,000 km² Mare Vaporum pyroclastic deposit. It exhibits higher TiO₂ contents (>10 wt%) than Sulpicius Gallus but a limited areal extent of H₂O/OH abundances <~200 ppm. The Clementine color ratio map shows slightly different spectral characteristics of both of these deposits compared to Rima Bode and Sinus Aestuum. The Mare Vaporum deposits have dark blue spectra more consistent with mare basalts, whereas Sulpicius Gallus exhibits reddish-purple coloration that may result from more mature mafic soils. While Sulpicius Gallus has good stereo imaging coverage, no stereo pairs are currently available for the Mare Vaporum deposit (Figure 2(c)). As a result, we have given Sulpicius Gallus a higher ranking than Mare Vaporum, and we rank Sulpicius Gallus just below Rima Bode. The volatile budget and volcanic evolution on the Moon can be addressed at Sulpicius Gallus via the same key measurements recommended by Jawin et al. (2019) for Rima Bode.

6.2. High-FeO/Low-TiO₂ Pyroclastics (Group 2)

The Aristarchus plateau contains the largest pyroclastic deposit on the Moon (Gaddis et al. 2003; Figure 3), with volatile contents of ≥300 ppm (Milliken & Li 2017). Jawin et al. (2019) summarized the relevance of this site for scientific themes, which includes the volcanic evolution and volatile budget of the Moon. Characterizing the composition and distribution of volatiles at this location would meet one of the NASA Decadal Survey objectives and address SKGs related to resource potential. Examination of Aristarchus materials would also provide mineralogical and compositional ground truthing

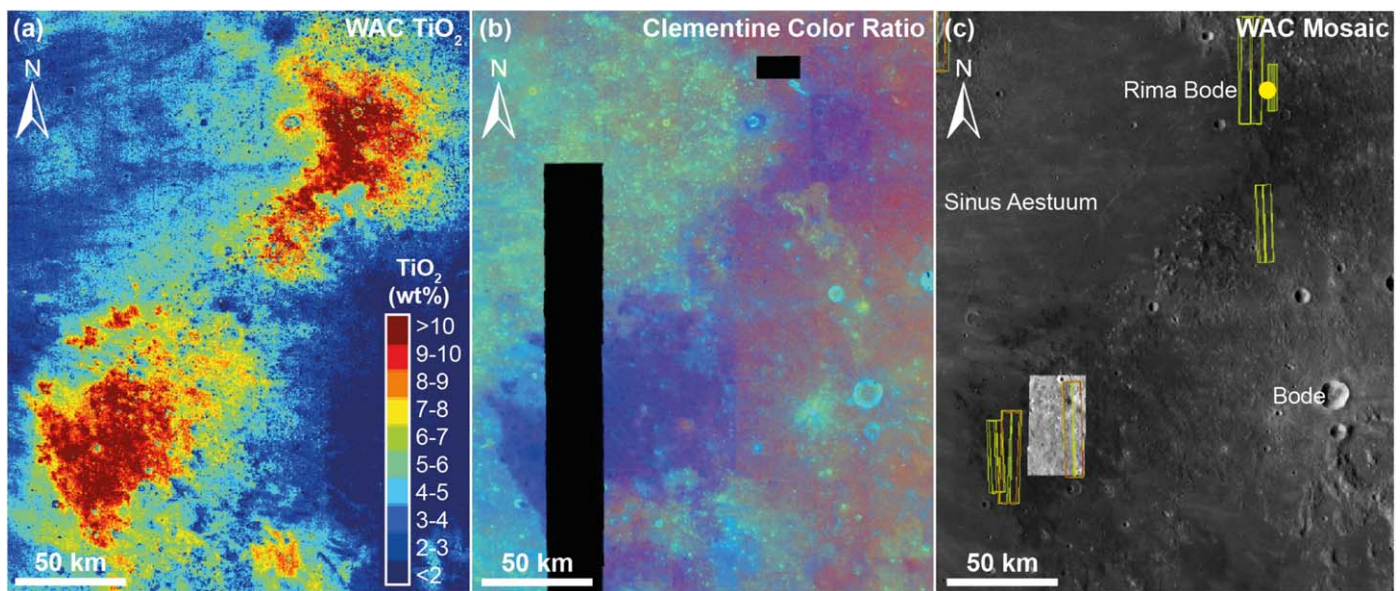


Figure 1. Rima Bode is to the northeast of other pyroclastic deposits in southern Sinus Aestuum. Both are potential ISRU characterization sites. (a) WAC color-derived TiO_2 map, (b) Clementine color ratio (McEwen et al. 1994; Pieters et al. 1994), and (c) locations of LRO NAC stereo observations (yellow boxes), DTMs (red boxes), the Constellation ROI (yellow dot), and controlled mosaics overlaid on the WAC mosaic. Data retrieved from LROC Quickmap (<https://quickmap.lroc.asu.edu>).

for regional pyroclastics with lower TiO_2 (<2 wt%) contents (Figure 3(a)) than at the Apollo 17 landing site (~ 7.5 wt%). Key measurements recommended by Jawin et al. (2019) for addressing the scientific themes include bulk chemistry and mineralogy, volatile contents, and quantification of geomechanical regolith properties. The NAC stereo coverage is available for the Aristarchus 2 and Rimae Prinz (Montes Harbinger) Constellation ROIs, as well as crossing Valles Schröteri. However, the coverage along Valles Schröteri also coincides with a weaker spectral signature of the pyroclastics due to overprinting by ejecta from the Aristarchus crater (Figures 3(b) and (c)). The high-iron, low-titanium spectral signature of the glasses is expressed in the Clementine color ratio as an orange spectral unit (Figure 3(b)).

We rank the Aristarchus 2 Constellation region (yellow dot to the southwest of the Aristarchus plateau label in Figure 3(c)) or another nearby area exhibiting the highest $\text{H}_2\text{O}/\text{OH}$ signatures as a preferred characterization region (Table 2). The indigenous water signal, while also showing areas with ≥ 300 ppm, is less areally extensive by the Rimae Prinz Constellation site, but there are a greater number of NAC stereo observations for this area available. Both areas should be examined in more detail for selection of specific characterization landing sites.

6.3. High- TiO_2 and/or High-FeO Basalts (Groups 3 and 4)

The ISRU techniques can also be tested and demonstrated using mare basalt regolith. Two mare types identified by Chevrel et al. (2002) contain high TiO_2 and FeO contents: M1 (6.0–7.0 wt% TiO_2 , 14.5–15.3 wt% FeO) and M2 (5.8–6.8 wt% TiO_2 , 14.9–15.7 wt% FeO). For our study, however, it was not possible to fully evaluate potential ISRU landing sites within the M5 type or the to-date-unsampled M2 basalt type, which is described as a science target by Flahaut et al. (2012) and Kring & Durda (2012). Additional work would be needed to assess the locations where the M2 spectral signature is associated with previously proposed mare basalt landing sites (e.g., northwestern Mare Tranquillitatis, east of Lichtenberg Crater) or to propose new sites for this

material. Nevertheless, exploration of these two locations in LROC Quickmap reveals that they generally exhibit larger rock abundances (Bandfield et al. 2011) and lower H -parameters or higher thermal inertia values (Hayne et al. 2017) than regional pyroclastic deposits. For example, an ~ 100 km² area in northwestern Tranquillitatis, exhibiting the highest TiO_2 content of the region, has a rock abundance of 0.005 and an H -parameter of 0.072 compared with a similar-sized area to the northwest of the Taurus Littrow valley that shows values of 0.003 and 0.075, respectively (Figure 4). An area around the Aristarchus 2 Constellation ROI (Figure 3) shows values of 0.003 and 0.076, respectively. Rock abundance values (0.006) at the mare deposit exhibiting the highest TiO_2 values east of the Lichtenberg crater are larger than in Mare Tranquillitatis, while the H -parameter is lower (0.068). These observations indicate greater overall rockiness at the surface and near surface at mare basalts of interest compared with pyroclastic deposits and translate to potentially greater hazards for landing, as well as the potential need for increased beneficiation of the materials for ISRU.

Using LRO Wide Angle Camera (WAC) color data, the new TiO_2 map (Sato et al. 2017) also allows a new look at the locations where lower- TiO_2 , high-FeO basalts are present. One suggested landing site for examining such materials is the young P60 basalt described in Hiesinger et al. (2003), Stadermann et al. (2018), and Jawin et al. (2019) and proposed as a science landing site by Draper et al. (2021). Here the FeO abundance derived from Clementine data (Lucy et al. 2000) is ~ 18 wt%, while the WAC-derived TiO_2 content (Sato et al. 2017) is ~ 6 wt%. Again, the rock abundance is larger and H -parameter lower compared to values at pyroclastic deposits at an area of the P60 basalt southwest of Aristarchus Crater, in the region of the proposed ISOCHRON landing site (Draper et al. 2021).

Thus, the regolith on basalt units appears less advantageous for the small-scale ISRU demonstration envisioned by ESA, because it tends to be rockier than pyroclastic deposits. Rocks and boulders would need to be removed or crushed prior to processing. At larger-scale operations, coherent flow units

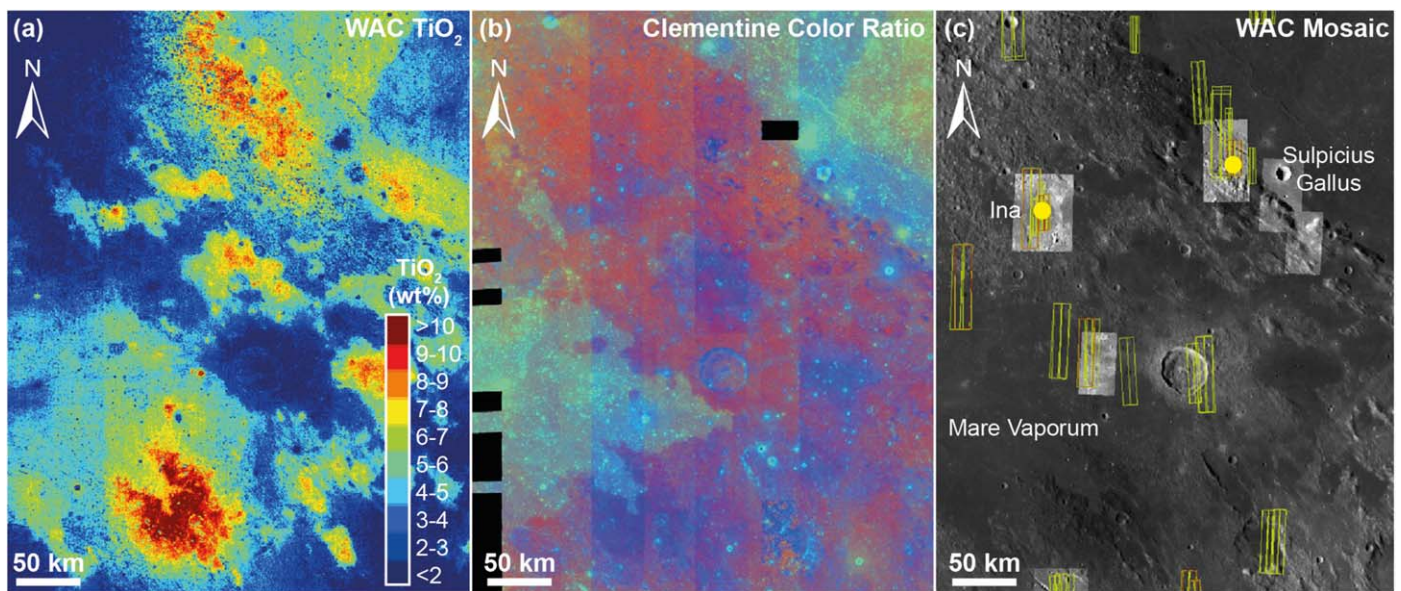


Figure 2. Sulpicius Gallus is north–northeast of the Mare Vaporum pyroclastic deposits. Both are potential ISRU characterization sites. (a) WAC color-derived TiO_2 map of Sato et al. (2017), (b) Clementine color ratio (McEwen et al. 1994; Pieters et al. 1994), and (c) locations of LRO NAC stereo observations (yellow boxes), DTMs (red boxes), Constellation ROIs (yellow dots), and controlled mosaics overlaid on the WAC mosaic. Data retrieved from LROC Quickmap (<https://quickmap.lroc.asu.edu>).

would require more work-intensive methods to excavate and beneficiate than unconsolidated pyroclastics (e.g., Crawford 2015; Lawrence & Hawke 2008; Just et al. 2020; Rasera et al. 2020). Nevertheless, a characterization mission sent to investigate the regolith, particularly at unsampled mare basalt types, would provide additional compositional and geomechanical information about the suitability of mare regolith as an ISRU feedstock.

6.4. Recommendations for ISRU Characterization Sites

The preliminary group of highest-ranked landing sites (the Aristarchus plateau, Montes Harbinger/Rimae Prinz, Rima Bode, and Sulpicius Gallus; Table 2 entries in bold) focuses on regional pyroclastic deposits that are accessible within the given engineering constraints. The Aristarchus plateau and adjacent Montes Harbinger/Rimae Prinz exhibit pyroclastic materials that have remotely sensed low-Ti, high- Fe^{2+} compositions that differ from the high-Ti materials at Rima Bode and Sulpicius Gallus. The latter two locations have remotely sensed Ti and Fe compositions similar to the regional pyroclastics northwest of the Apollo 17 landing site (e.g., Gaddis et al. 2003). Thus, selection of a site on the Aristarchus plateau would allow the characterization of previously uncharacterized materials, whereas a mission to Rima Bode or Sulpicius Gallus would allow a comparison of the similarity of these materials to Apollo 17 samples. Characterization at any of these sites would allow the evaluation of the reported high concentrations of indigenous water in some pyroclastic deposits (Milliken & Li 2017). Based on the studies presented in Jawin et al. (2019), key measurements of bulk chemistry and mineralogy, volatile contents, and quantification of geomechanical regolith properties would address both scientific themes and SKGs for potential ISRU materials. The planned characterization package contains instruments that match these recommendations.

The next steps to support the achievement of the ISRU characterization goals from the landing site selection perspective include (1) processing, calibration, and map projection of the

relevant data sets in ArcGIS; (2) geological mapping of the ROIs; (3) analysis of the spectral properties of the units; (4) hazard and terrain assessment; (5) evaluation of local illumination conditions; and (6) selection of specific landing sites based on more detailed engineering constraints for both the lander and equipment.

7. Potential ISRU E2E Demonstration Site

The most complete information for the local characteristics of lunar regolith comes from Apollo and Luna sample studies, in particular for the Apollo 15–17 landing sites, where an improved drive tube design allowed better collection of the cores (e.g., Carrier et al. 1991). While remote-sensing data can provide a global view of the range and variation of different properties, their results are model-based. Thus, for selection of an E2E demonstration landing site, we focus on landing site recommendations near prior landing sites to increase the likelihood of having predictable regolith characteristics for a one-step ISRU demonstration mission. We examined and selected an area that is on a geological unit that is interpreted to be the same as or similar to units at the Apollo 17 landing site using geological maps, as described below.

7.1. A Southeast Mare Serenitatis ISRU E2E Demonstration Site

The Apollo 17 mission visited the Taurus Littrow valley ($20^\circ 2\text{N}$, $30^\circ 8\text{E}$) at the edge of southeastern Mare Serenitatis (National Aeronautics and Space Administration 1973). The goal was to investigate the highland massifs, basalt deposits, and dark mantle deposit (Figure 4(a)). The regolith at the landing site is about 15 m thick, and the dark mantling deposits were determined to contain orange and black glass (Muehlberger et al. 1973; Schmitt & Cernan 1973; Hiesinger & Head 2006; Schmitt et al. 2017). The Apollo soil samples themselves exhibit 2%–20% proportions of glass beads (Heiken & McKay 1974). The black glass beads contain crystallized ilmenite and olivine, in contrast to the orange beads, which are primarily quenched glass (e.g.,

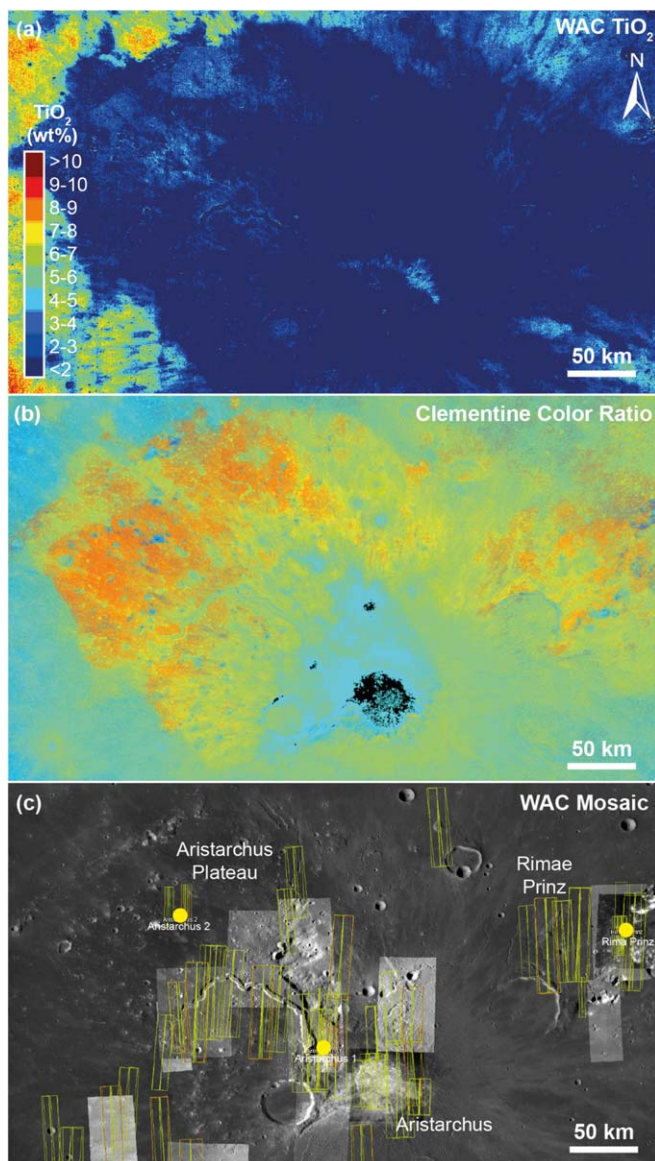


Figure 3. Aristarchus plateau and Rimae Prinz regions are Constellation program ROIs and potential ISRU characterization sites. (a) WAC color-derived TiO_2 map of Sato et al. (2017), (b) Clementine color ratio (McEwen et al. 1994; Pieters et al. 1994), and (c) locations of LRO NAC stereo observations (yellow boxes), DTMs (red boxes), Constellation ROIs (yellow dots), and controlled mosaics overlaid on the WAC mosaic. Data retrieved from LROC Quickmap (<https://quickmap.lroc.asu.edu>).

Heiken & McKay 1974; Arndt & von Engelhardt 1987). The orange glass has compositions with $\sim 8\text{--}10$ wt% TiO_2 and $\sim 21\text{--}23$ wt% FeO (Delano & Lindsley 1983). Soils with orange and black glass also exhibit identical compositional characteristics (~ 9 wt% TiO_2 , $\sim 22\text{--}23$ wt% FeO; Blanchard & Budahn 1978); thus, it has been concluded that the glass cooling rate history and crystallinity lead to the glass beads/soils differing appearance, rather than compositional differences (Heiken & McKay 1974).

Thus, we studied the region south of Clerke Crater (Figure 4(a)) to find potential landing sites for an E2E ISRU demonstration mission for two reasons: (1) the proximity to the Apollo 17 landing site allows extrapolation of known physical and compositional characteristics of the pyroclastic materials and regolith in the Taurus Littrow valley to the nearby pyroclastic deposit south of Clerke Crater, and (2) an ilmenite- and Ti-rich pyroclastic deposit

would allow testing of both hydrogen and methane reduction oxygen extraction, as well as the FFC Cambridge method. We compiled numerous lunar data sets within a geographic information system to allow the selection of potential landing sites on the basis of composition, illumination conditions, and hazard considerations, including slope and rock abundance (Figures 4–7).

7.1.1. Regional Characteristics

The region south of Clerke Crater is covered by a suite of camera data ranging from complete coverage by the LRO WAC (100 m pixel^{-1} ; Robinson et al. 2010; Figure 4(a)) and SELENE Terrain Camera (TC; $\sim 7\text{ m pixel}^{-1}$; Haruyama et al. 2008; Figure 4(b)) to partial coverage by the LRO NAC ($<0.5\text{ m pixel}^{-1}$; Robinson et al. 2010; Figure 4(c)). These image products augment legacy data sets that were used to plan the Apollo 17 mission. A WAC-based crater size–frequency distribution (CSFD) measurement indicates that the pyroclastic deposits in this region have an age of ~ 3.66 Ga (van der Bogert et al. 2016), which is consistent with work by Hiesinger et al. (2000) on Lunar Orbiter data that give an age of 3.70 ± 0.4 Ga for the Taurus Littrow valley and $3.81 + 0.03\text{--}0.05$ Ga for the unit surrounding Clerke Crater. A TC-based age determination south of Clerke Crater indicates the presence of two different layered deposits with ages of ~ 3.63 and ~ 3.83 Ga (van der Bogert et al. 2016). Because two discrete ages can be derived from this CSFD, a thickness for the younger deposit can be determined using the method of Hiesinger et al. (2002) and is thus estimated to be $\sim 26\text{--}40$ m thick (van der Bogert et al. 2016). This is consistent with the inferred thickening of the pyroclastics deposit to the west of the Apollo 17 landing site by other workers (Wolfe et al. 1975; Heiken et al. 1974), including results from radar observations (Carter et al. 2009).

These Earth-based S-band radar observations (Campbell et al. 2007) also suggest that the pyroclastic deposits in this region have no large rocks ($\sim 1\text{--}50$ cm in diameter) for at least 1–5 m depth (Figure 4(d); Zisk et al. 1974; Thompson 1979; Carter et al. 2009). A low rock abundance (~ 0.003) is also apparent in the Diviner rock abundance map (Figure 4(e); Bandfield et al. 2011), where a higher rock abundance is generally related to steep crater rims. The thermal inertia of the dark mantle deposit is extremely low, with H -parameter values (~ 0.075 and higher) approaching their maximum (Hayne et al. 2017; Figure 4(f)). Only fresh craters show higher thermal inertias.

The Clementine color ratio (Figure 5(a)) shows an extremely dark purplish-blue signature associated with the dark mantle deposit, which is interpreted as a large regional pyroclastic deposit (e.g., Gaddis et al. 1985, 2000; McEwen et al. 1994; Pieters et al. 1994). The pyroclastic deposit is characterized by high FeO ($\sim 20\%$; Lucey et al. 2000; Figure 5(b)) and TiO_2 ($>10\%$; Sato et al. 2017; Figure 5(c)) contents. The highly mafic signature of the pyroclastic deposit is also seen in the high values shown in the Christiansen feature map (Greenhagen et al. 2010; Figure 5(d)). Thus, the compositions in the dark mantle deposit are ideal for hydrogen reduction ISRU (e.g., Hawke et al. 1990) and would also be suitable for methane reduction and FFC Cambridge techniques. These data can be used to define a region that has a highly mafic signature with high ilmenite contents (Figure 5(e)).

Geological maps of this region were made in preparation for the Apollo 17 mission (e.g., Scott & Carr 1972; Lucchitta 1972). The map of Scott & Carr (1972) shows a geographically

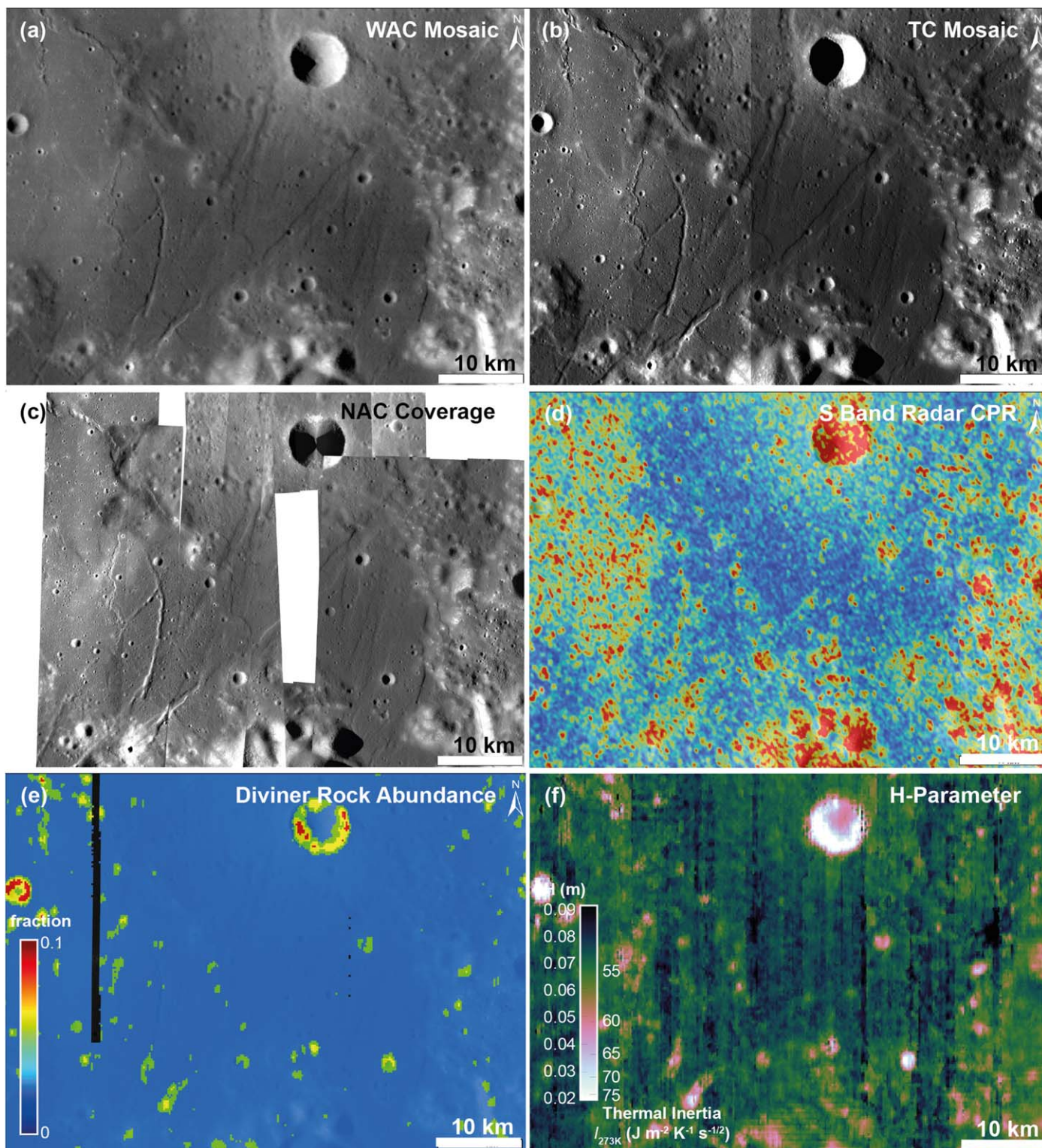


Figure 4. Image data, radar, and Diviner data for southeast Mare Serenitatis. (a) LRO WAC mosaic (100 m pixel^{-1}), (b) SELENE TC mosaic ($\sim 7 \text{ m pixel}^{-1}$), (c) LRO NAC coverage ($\sim 0.5 \text{ m pixel}^{-1}$), (d) Earth-based S-band radar cross-polarization ratio map, (e) Diviner rock abundance, and (f) H -parameter or thermal inertia. See Section 7.1.1 for data sources.

extensive dark mantle (pyroclastic) deposit in southeast Mare Serenitatis and extending into the Taurus Littrow valley to the southeast. Iqbal et al. (2019) prepared a new geological map for this region using modern lunar remote-sensing data (Figure 5(f)). It shows the extensive dark mantle deposit in green. There are a series of northeast-to-southwest trending graben (black lines) that

potentially represent hazards for a lander due to their higher slopes at the fault traces. Closer to Clerke Crater, materials from underneath the pyroclastic deposits have been excavated and mixed into the Clerke ejecta deposits.

To evaluate the slopes and illumination conditions within this region, a selection of topographic data is available. The

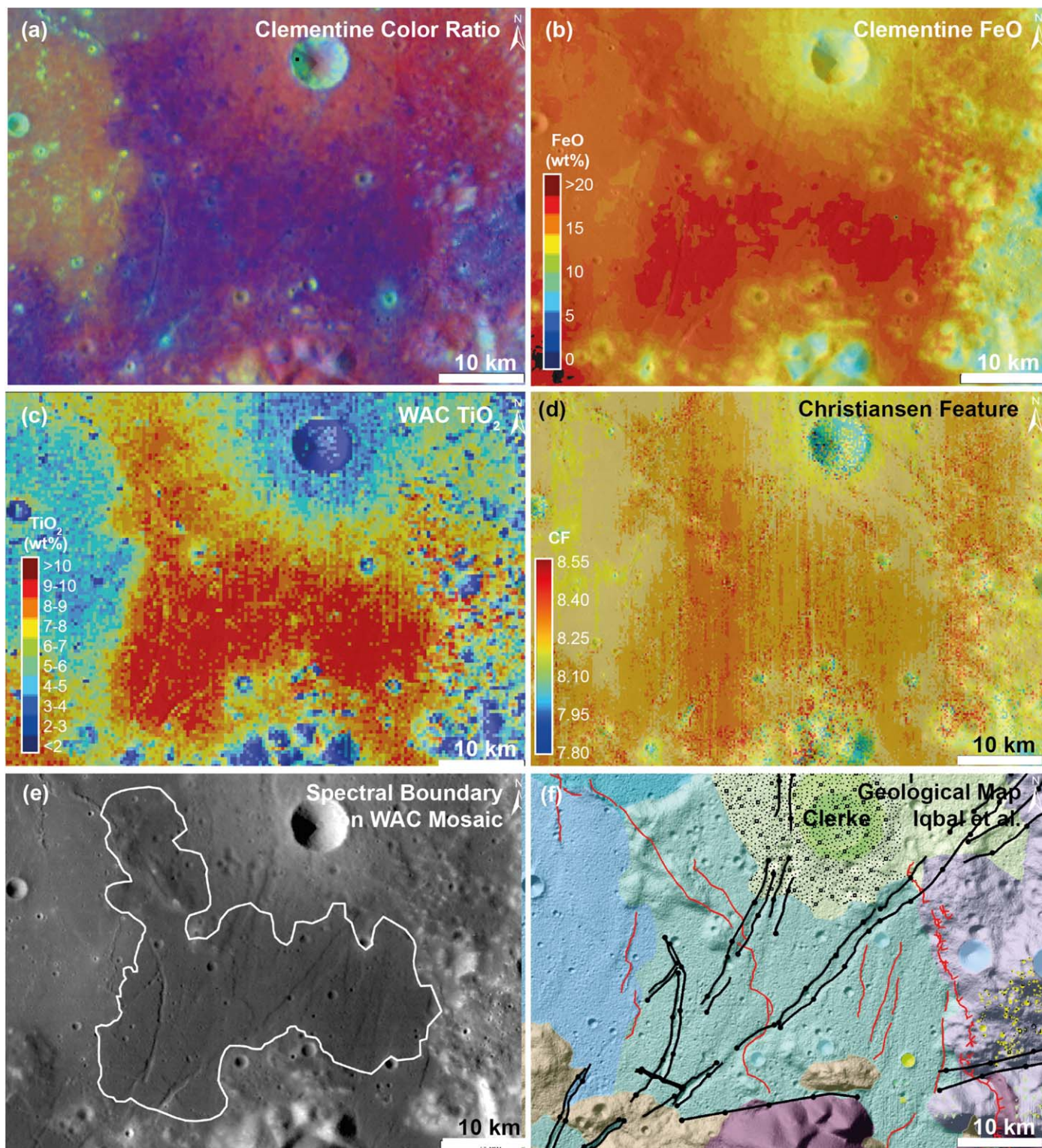


Figure 5. Spectral data and resource boundary mapping for southeast Mare Serenitatis. Shown are the (a) Clementine color ratio composite map; (b) Clementine FeO map (c) WAC TiO₂; (d) Diviner Christiansen feature map; (e) mapped approximate boundary map of the maximum Fe and Ti concentrations; and (f) preliminary new geological map of the region showing widespread dark mantle material (green). See Section 7.1.1 for data sources.

WAC GLD 100 DTM ($\sim 100 \text{ m pixel}^{-1}$; Scholten et al. 2012) provides a large-scale overview of the region with baselines of about 300 m. The LOLA/Kaguya Merge DTM (512 ppd; Figure 6(a)) provides slightly higher-resolution topographic information with a baseline of about 67 m pixel^{-1} (Barker et al. 2016). High-resolution DTMs derived from NAC stereo

images are only available for limited locations. Figure 6(b) shows the current available coverage in southeast Mare Serenitatis. Due to the need for high-resolution topographic information for landing site safety, current selection of a landing site would be limited to the area with NAC DTM coverage.

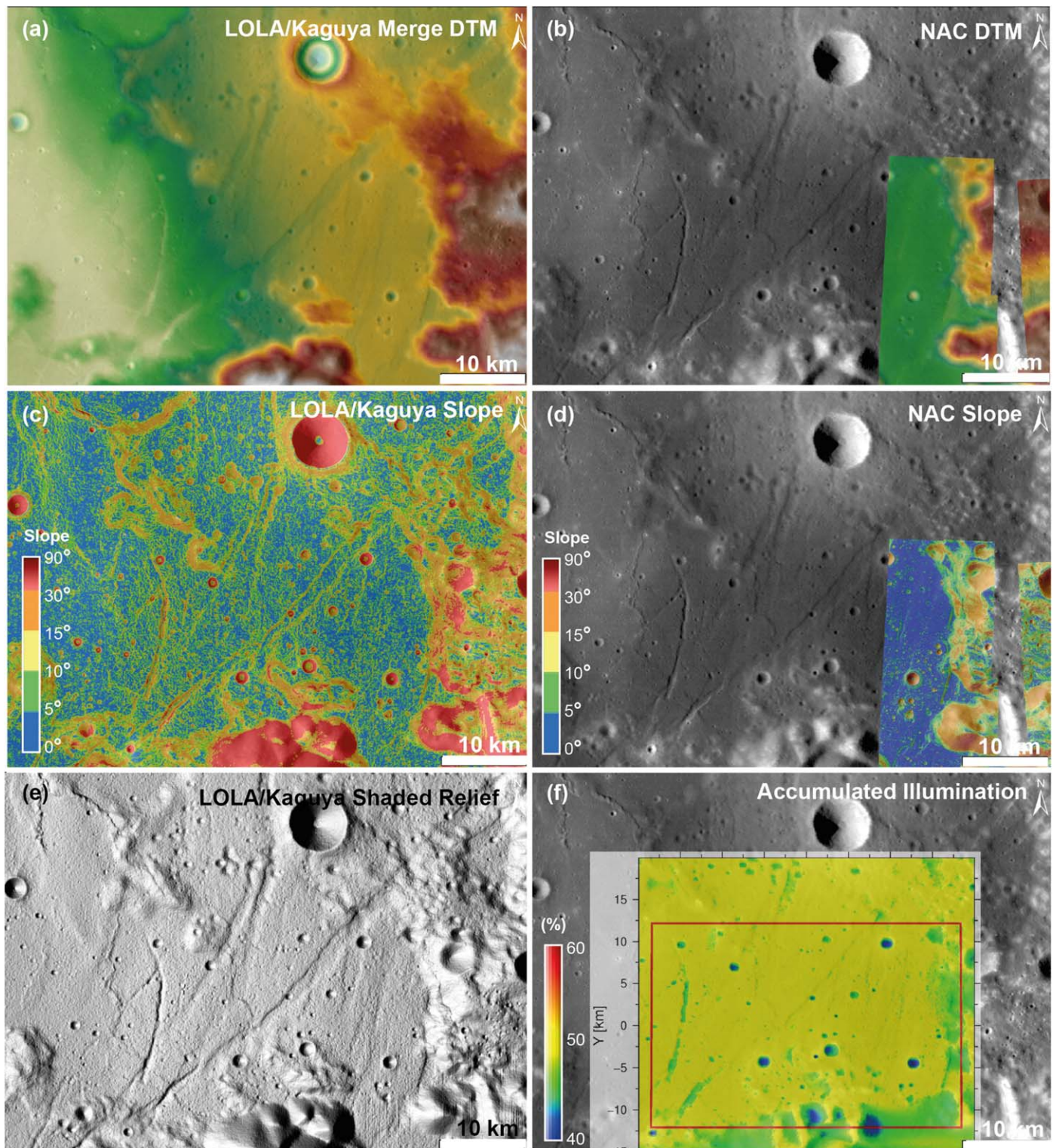


Figure 6. Topographic data plus derived slope and accumulated illumination for southeastern Mare Serenitatis. (a) LOLA/Kaguya merged DTM, (b) DTM coverage derived from NAC stereo imaging, (c) LOLA/Kaguya merge DTM slope map, (d) NAC DTM slope map, (e) shaded relief map generated from the LOLA/Kaguya merge DTM, and (f) accumulated illumination in the region calculated from the LOLA/Kaguya DTM. See Section 7.1.1 for data sources.

The DTMs are used to generate higher-level products, such as slope maps (Figures 6(c) and (d)) and a shaded relief map (Figure 6(e)). The slope maps show that the dark mantle region in southeast Mare Serenitatis is generally very flat, with the exception of graben and impact craters. For our analysis, we also used the LOLA/Kaguya merge DTM (Barker et al. 2016)

to calculate the accumulated solar insolation in the ROI for a notional lunar day (Figure 6(f)). The map shows the percentage of time of illumination over one lunar day (terrestrial month). Areas in the easternmost portions of the pyroclastic deposit have slightly lower accumulated illumination because of long shadows cast by the massifs to the east. Some larger, deeper

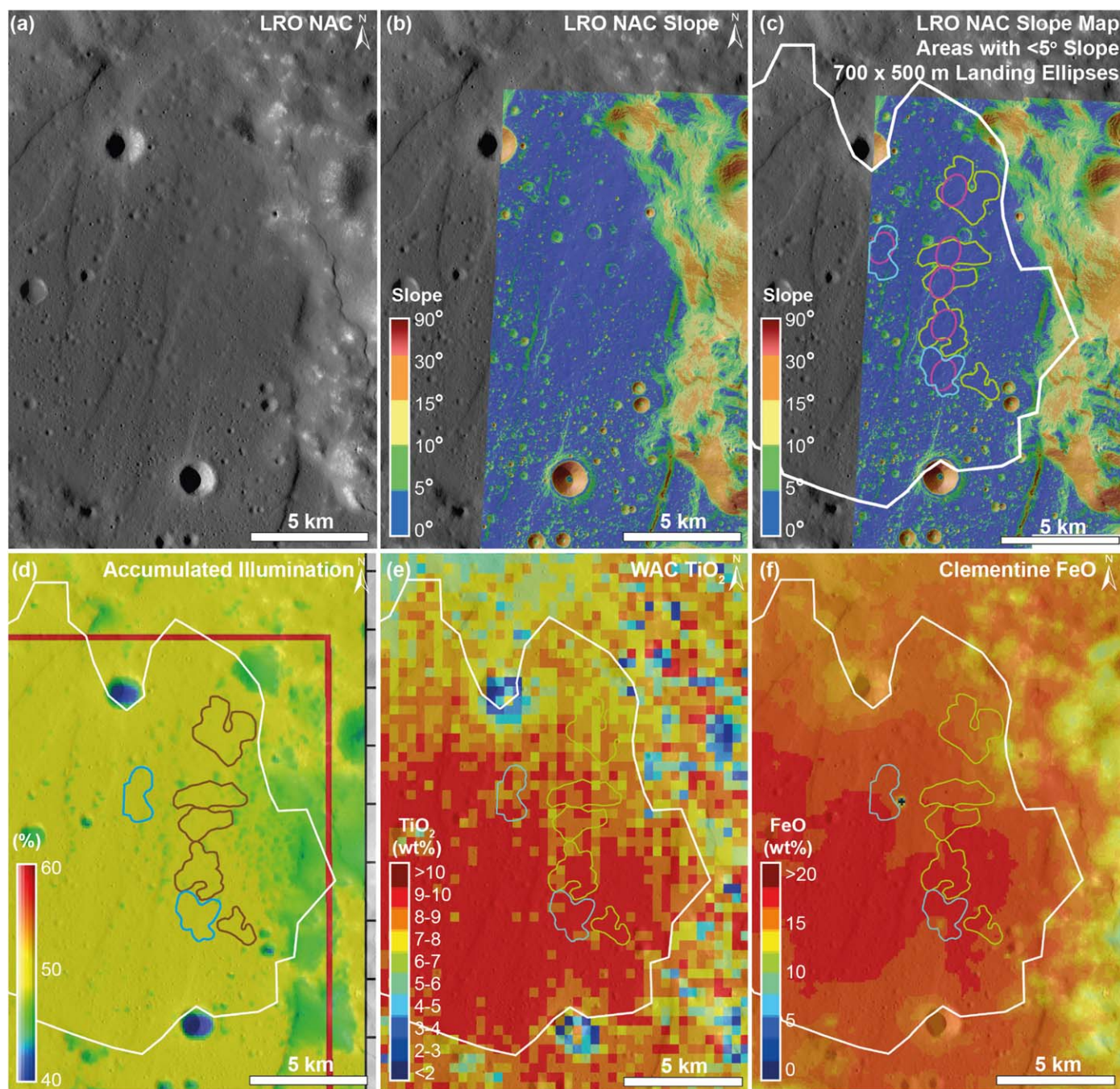


Figure 7. Imaging, topographic, and compositional information used to define two notional landing sites for E2E ISRU demonstration in southeastern Mare Serenitatis. (a) LRO NAC image coverage. (b) LRO NAC slope map generated from the NAC DTM. (c) Mapped locations with the largest continuous areas with slopes $<5^\circ$ and notional 700×500 m landing ellipses (pink), where the cyan areas have more favorable illumination conditions, as shown in panel (d), accumulated solar insolation calculated from the LOLA/Kaguya merge DTM for a random lunar day. The compositional maps showing both Ti and Fe compositions, (e) LRO WAC TiO₂ and (f) Clementine FeO, allow selection of sites with optimized safety, illumination, and compositional characteristics. The southernmost cyan area contains the highest FeO and TiO₂ contents with low slopes and maximum solar insolation.

craters also exhibit $\sim 40\%$ accumulated insolation, compared with 50% (~ 14 days) on flat, smooth areas.

7.1.2. Local Characteristics/Site Selection

More detailed landing site recommendations can be made on the basis of high-resolution data. Figures 7(a) and (b) show the coverage by LRO NAC imagery and the slope map derived from a DTM generated from available NAC stereo images. Using this map and building on the work discussed in the previous sections,

contiguous areas with slopes of $<5^\circ$ were mapped (green and cyan in Figure 7(c)). These areas also exhibit low rock abundance values. The cyan marked areas represent locations where the accumulated solar insolation is greatest at up to 50% (Figure 7(d)). The WAC TiO₂ (up to >10 wt%; Figure 7(e)) and Clementine FeO values (up to >20 wt%; Figure 7(f)) are greatest in the southernmost cyan area, indicating that a landing site within this region would give potentially the greatest ilmenite content of areas also exhibiting slopes of $<5^\circ$, low rock abundance, and $\sim 50\%$ (the maximum) accumulated solar insolation. Therefore, if a

landing site is selected using the currently available data, we would recommend a location within the southernmost cyan area.

The next steps for the analysis of hazards for this possible landing region should include the examination of very high incidence angle NAC images (to better assess the presence of small boulders based on casting of long shadows). Crater and boulder size–frequency measurements for small craters (<~50 m) and boulders (<~20 m) would provide additional information for hazard avoidance planning and pinpointing a landing site within the selected area. A detailed analysis of the terrain characteristics via a TRI would also augment hazard assessment. Finally, once the landing date is known, the solar insolation calculations can be updated for the specific time period of surface operations.

8. Summary and Conclusions

Much is known about the properties and compositions of the lunar regolith from the Apollo and Luna landed missions. However, there are many uncharacterized regions of the Moon, which may represent useful deposits for oxygen extraction via ISRU. In this study, we reviewed such regions in the scope of “characterization sites,” where additional information about the compositional and physical properties of the materials is required to assess the usefulness of the deposits for ISRU, as well as to investigate their similarities to or differences from known resources. The preliminary group of highest-ranked landing sites (the Aristarchus plateau, Montes Harbinger/Rimae Prinz, Sulpicius Gallus, and Rima Bode) focuses on regional pyroclastic deposits that are accessible within the given engineering constraints. The Aristarchus plateau and adjacent Montes Harbinger/Rimae Prinz exhibit pyroclastic materials that have remotely sensed low-Ti, high-Fe²⁺ compositions that differ from the high-Ti materials at Rima Bode and Sulpicius Gallus. The latter two locations have remotely sensed compositions similar to the regional pyroclastics northwest of the Apollo 17 landing site. As such, the selection of a site on the Aristarchus plateau would allow the investigation of previously uncharacterized materials, whereas a mission to Rima Bode or Sulpicius Gallus would allow comparison of these materials to those at the Apollo 17 landing site. Characterization at any of these sites would allow the evaluation of the reported high concentrations of indigenous water in some pyroclastic deposits.

For a stand-alone E2E ISRU demonstration mission, a fuller understanding of the physical and compositional characteristics of the resource deposits is required to reduce the overall risk for the demonstration. Thus, we examined locations near several prior Apollo and Luna landing sites as potential E2E test sites to allow extrapolation of ground-truth information to nearby deposits. Because a Ti-rich pyroclastic deposit seems to be advantageous from both beneficiation and compositional perspectives, we examined an example landing site for an E2E demonstration to the northwest of the Taurus Littrow valley, south of Clerke Crater. Both hydrogen and methane reduction techniques could be tested here, as well as the FFC Cambridge method. We mapped landing regions that would maximize both the Ti and Fe contents of the regolith, as well as offering slopes of <5° and accumulated illumination approaching 50% (~14 days). The next steps for selecting a landing site within this region would be to examine low Sun (high incidence angle) NAC images for identification of hazardous boulders and/or craters, as well as performing additional crater and boulder size–frequency analyses. Final site selection can also be optimized with additional input from the lander providers and engineers regarding the mission design.

We thank Erick Malaret and his team for developing LROC Quickmap as a transformative, flexible, and multifaceted tool for examining numerous georeferenced lunar data sets. Given the constraints of the standard rainbow color maps presented here and in the original publications for certain data sets, Quickmap (<https://quickmap.lroc.asu.edu>) also makes it possible to explore many of the data sets with alternate color maps and scales to increase data accessibility. We thank the two reviewers for their comments and suggestions for helpful improvements to the paper. C.H.v.d.B., H.H., and A.L. were supported by an OHB Italia subcontract during the ESA Commercial ISRU Demonstration Mission Preparation Phase. C.H.v.d.B. and H.H. were also supported by German Aerospace Center (Deutsches Zentrum für Luft- und Raumfahrt) projects 500W1504 and 500W2001. P.G. was supported by German Research Foundation (Deutsche Forschungsgemeinschaft—DFG) grant GJ865/2-1.

ORCID iDs

Carolyn H. van der Bogert  <https://orcid.org/0000-0003-2882-7037>

References

- Allen, C. C., Morris, R. V., & McKay, D. S. 1996, *JGRE*, **101**, 26085
- Anand, M., Crawford, I. A., Balat-Pichelin, M., et al. 2012, *P&SS*, **74**, 42
- Arndt, J., & von Engelhardt, W. 1987, *JGR*, **92**, E372
- Bandfield, J. L., Ghent, R. R., Vasavada, A. R., et al. 2011, *JGR*, **116**, E00H02
- Barker, M. K., Mazarico, E., Neumann, G. A., et al. 2016, *Icar*, **273**, 346
- Bauch, K. E., Hiesinger, H., Helbert, J., Robinson, M. S., & Scholten, F. 2014, *P&SS*, **101**, 27
- Bennett, N. J., Ellender, D., & Dempster, A. G. 2020, *P&SS*, **182**, 104842
- Bibring, J.-P., Hamm, V., Pilorget, C., Vago, J. L. & and the MicrOmega team 2017, *AsBio*, **17**, 621
- Binns, D. A., Hufenbach, B., Borggräfe, A., et al. 2018, in IAF Space Exploration Envelope Symp., 69 (Paris: IAF), 46742, <https://iafastro.directory/iaac/paper/id/46742/summary/>
- Biswas, J., Sheridan, S., Pitcher, C., et al. 2020, *P&SS*, **181**, 104826
- Blanchard, D. P., & Budahn, J. R. 1978, *LPSC*, **9**, 1969
- Campbell, B. A., Campbell, D. B., Margot, J. L., et al. 2007, *ITGRS*, **45**, 4032
- Carpenter, J., Fisackerly, R., & Houdou, B. 2016, *SpPol*, **37**, 52
- Carpenter, J. D., Fisackerly, R., De Rosa, D., & Houdou, B. 2012, *P&SS*, **74**, 208
- Carrier, W. D., III 1973, *Moon*, **6**, 250
- Carrier, W. D., III 1974, *Moon*, **10**, 183
- Carrier, W. D., III 2003, *J. Geotech. Geoenviron. Eng.*, 129, 956
- Carrier, W. D., III 2005, The Four Things You Need to Know About the Geotechnical Properties of Lunar Soil, https://www.lpi.usra.edu/lunar/surface/carrier_lunar_soils.pdf.
- Carrier, W. D., III, Olheoft, G. R., & Mendell, W. 1991, in Lunar Sourcebook, ed. G. H. Heiken, D. T. Vaniman, & B. M. French (Cambridge: Cambridge Univ. Press), 475
- Carter, L. M., Campbell, B. A., Hawke, B. R., Campbell, D. B., & Nolan, M. C. 2009, *JGRE*, **114**, E11004
- Chevrel, S. D., Pinet, P. C., Daydou, Y., et al. 2002, *JGRE*, **107**, 5132
- Cooper, B. 2007, in The Moon—Resources, Future Development and Settlement, ed. D. Schunk et al. (Berlin: Praxis, Springer), 261
- Crawford, I. A. 2015, *PrPG*, **39**, 137
- Cutler, A. H., & Krag, P. 1985, in Lunar Bases and Space Activities for the 21st Century, ed. W. W. Mendell (Houston, TX: Lunar and Planetary Institute), 559
- Delano, J. W. 1986, *JGR*, **91**, D201
- Delano, J. W., & Lindsley, D. H. 1983, *JGRS*, **88**, B3
- Draper, D. S., Lawrence, S. J., Klima, R. S., et al. 2021, *PSJ*, **2**, 79
- European Space Agency 2019a, ESA Strategy for Science at the Moon, <https://exploration.esa.int/s/WmMyaoW>
- European Space Agency 2019b, ESA Space Resources Strategy, <https://exploration.esa.int/s/WyP6RXw>
- Flahaut, J., Blanchette-Guertin, J.-F., Jilly, C., et al. 2012, *AdSpR*, **50**, 1647
- Gaddis, L. R., Hawke, B. R., Robinson, M. S., & Coombs, C. 2000, *JGR*, **105**, 4245
- Gaddis, L. R., Pieters, C. M., & Hawke, B. R. 1985, *Icar*, **61**, 461

- Gaddis, L. R., Staid, M. I., Tyburczy, J. A., Hawke, B. R., & Petro, N. E. 2003, *Icar*, **161**, 262
- Gläser, P., & Gläser, D. 2019, *A&A*, **627**, A129
- Gläser, P., Oberst, J., Neumann, G. A., et al. 2018, *P&SS*, **162**, 170
- Graf, J. C. 1993, Lunar Soils Grain Size Catalog (Houston, TX: NASA), 488
- Greenhagen, B. T., Lucey, P. G., Wyatt, M. B., et al. 2010, *Sci*, **329**, 1507
- Gruener, J. E. 2009, in NASA Constellation Program Office Regions of Interest on the Moon: An Update for the 2009 Annual Meeting of the Lunar Exploration and Analysis Group, https://www.lpi.usra.edu/meetings/leag2009/presentations/Day-2%20PM/03-35_Gruener.pdf
- Haruyama, J., Matsunaga, T., Ohtake, M., et al. 2008, *EP&S*, **60**, 243
- Hawke, B. R., Coombs, C. R., & Clark, B. 1990, *LPSC*, **20**, 249
- Hayne, P. O., Bandfield, J. L., Siegler, M. A., et al. 2017, *JGR*, **122**, 2371
- Heiken, G., & McKay, D. S. 1974, *LPSC*, **5**, 843
- Heiken, G. H., McKay, D. S., & Brown, R. W. 1974, *GeCoA*, **38**, 1705
- Hiesinger, H., & Head, J. W. 2006, *RvMG*, **60**, 1
- Hiesinger, H., Head, J. W., Wolf, U., Jaumann, R., & Neukum, G. 2003, *JGRE*, **108**, 5065
- Hiesinger, H., Head, J. W., III, Wolf, U., Jaumann, R., & Neukum, G. 2002, *GeoRL*, **29**, 1248
- Hiesinger, H., Jaumann, R., Neukum, G., & Head, J. W. 2000, *JGR*, **105**, 29239
- Iqbal, W., Hiesinger, H., & van der Bogert, C. H. 2019, *LPSC*, **50**, 1005
- Jawin, E. R., Valencia, S. N., Watkins, R. N., et al. 2019, *E&SS*, **6**, 2
- Just, G. H., Smith, K., Joy, K. H., & Roy, M. J. 2020, *P&SS*, **180**, 104746
- Keller, J. W., Petro, N. E., Vondrak, R. R. & and the LRO team 2016, *Icar*, **273**, 2
- Kornuta, D., Abbud-Madrid, A., Atkinson, J., et al. 2018, Commercial Lunar Propellant Architecture—A Collaborative Study of Lunar Propellant Production, https://www.lpi.usra.edu/lpi/contribution_docs/LPI-002142.pdf
- Kring, D. A., & Durda, D. D. 2012, *LPICo*, 1694, <https://www.lpi.usra.edu/exploration/CLSE-landing-site-study/>
- Lawrence, S. J., & Hawke, B. R. 2008, *LPSC*, **39**, 1804
- Lindsay, J. 1976, in Lunar Stratigraphy and Sedimentology, ed. Z. Kopal & A. G. W. Cameron (Amsterdam: Elsevier)
- Lomax, B. A., Conti, M., Khan, N., et al. 2020, *P&SS*, **180**, 104748
- Lucchitta, B. K. 1972, Geological map of part of the Taurus-Littrow region of the Moon, USGS Map I-800-2, https://www.lpi.usra.edu/resources/mapcatalog/usgs/I800_2/
- Lucey, P. G., Blewett, D. T., & Jolliff, B. L. 2000, *JGR*, **105**, 20297
- Lucey, P. G., Hawke, B. R., Pieters, C. M., Head, J. W., & McCord, T. B. 1986, *JGR*, **91**, D334
- Lunar Exploration Analysis Group (LEAG) 2016, Lunar Human Exploration Strategic Knowledge Gap Special Action Team Review, <https://www.nasa.gov/sites/default/files/atoms/files/leag-gap-review-sat-2016-v2.pdf>
- Lunar Exploration Analysis Group (LEAG) 2017, 69, Advancing the Science of the Moon: Report of the Lunar Exploration Analysis Group Special Action Team, <https://www.lpi.usra.edu/leag/reports/ASM-SAT-Report-final.pdf>
- McEwen, A. S., Robinson, M. S., Eliason, E. M., et al. 1994, *Sci*, **266**, 1858
- McKay, D. S., Heiken, G., Basu, A., et al. 1991, in Lunar Sourcebook, ed. G. H. Heiken, D. T. Vaniman, & B. M. French (Cambridge: Cambridge Univ. Press), 285
- Mendell, W. W. (ed.) 1985, Lunar Bases and Space Activities for the 21st Century (Houston, TX: Lunar and Planetary Institute), 866
- Meurisse, A., & Carpenter, J. 2019, ESA Activities as Support to ISRU Technology Development, Developing a New Space Economy, 5006, <https://www.hou.usra.edu/meetings/lunarlsru2019/>
- Meurisse, A., & Carpenter, J. 2020, *P&SS*, **182**, 104853
- Milliken, R. E., & Li, S. 2017, *NatGe*, **10**, 561
- Morris, R. V., Score, R., Dardano, C., & Heiken, G. 1983, NASA Johnson Space Center, 1183, <https://www.lpi.usra.edu/lunar/samples/LunarSoils.pdf>
- Muehlberger, W. R., Batson, R. M., Cernan, E. A., et al. 1973, Apollo 17: Preliminary Science Report. *NASA SP-330*
- National Aeronautics and Space Administration Scientific and Technical Information Office 1973, Apollo 17 Preliminary Science Report, *NASA SP-330*, <https://www.hq.nasa.gov/alsj/a17/a17psr.html>
- National Research Council (NRC) 2007, The Scientific Context for the Exploration of the Moon (Washington, DC: National Academies Press)
- National Research Council (NRC) 2011, Vision and Voyages for Planetary Science in the Decade 2011-2022 (Washington, DC: National Academies Press)
- National Aeronautics and Space Administration 2016, 2017, Strategic Knowledge Gaps (SKGs), <https://www.nasa.gov/exploration/library/skg.html>
- National Aeronautics and Space Administration 2020, NASA Technology Taxonomy, <https://www.nasa.gov/offices/oct/taxonomy/index.html>
- Pieters, C. M., Staid, M. I., Fischer, E. M., Tompkins, S., & He, G. 1994, *Sci*, **266**, 1844
- Preto, I., Freddi, R., Venditti, F., et al. 2020, in Lunar ISRU Demonstration Mission Phase-A: Payload for Extraction of Oxygen from the Regolith, 112, <https://els2020.arc.nasa.gov/abstracts>
- Rasera, J. N., Cilliers, J. J., Lamamy, J. A., & Hadler, K. 2020, *P&SS*, **186**, 104879
- Reiss, P., Kersch, F., & Grill, L. 2020, *P&SS*, **181**, 104795
- Rice, E. E., Hermes, P. A., & Musbah, O. A. 1997, in 35th AIAA Meeting Papers (Reston, VA: AIAA), 97
- Robinson, M. S., Brylow, S. M., Tschimmel, M., et al. 2010, *SSRv*, **150**, 81
- Sanders, G. B., & Larson, W. E. 2015, *AdSpR*, **55**, 2381
- Sargent, H. M., Abernathy, F. A. J., Barber, S. J., et al. 2020, *P&SS*, **180**, 104751
- Sato, H., Robinson, M. S., Lawrence, S. J., et al. 2017, *Icar*, **296**, 216
- Schlüter, L., & Cowley, A. 2020, *P&SS*, **181**, 104753
- Schmitt, H. H., & Cernan, E. A. 1973, A Geological Investigation of the Taurus-Littrow Valley, Apollo 17 Preliminary Science Report, *NASA SP-330*, 5-1
- Schmitt, H. H., Petro, N. E., Wells, R. A., et al. 2017, *Icar*, **298**, 2
- Scholten, F., Oberst, J., Matz, K.-D., et al. 2012, *JGR*, **117**, E00H17
- Schrunk, D. G., Sharpe, B. L., Cooper, B. L., & Thangavelu, M. 2008, The Moon: Resources, Future Development, and Settlement (Chichester: Praxis Publishing Ltd.), 561
- Schwandt, C., Hamilton, J. A., Fray, D. J., & Crawford, I. A. 2012, *P&SS*, **74**, 49
- Scott, D. H., & Carr, M. H. 1972, Geological Map of the Taurus-Littrow Region of the Moon: Apollo 17 Pre-mission Map, USGS Map I-800-1, https://www.lpi.usra.edu/resources/mapcatalog/usgs/I800_1/
- Simon, S. B., Papike, J. J., & Laul, J. C. 1981, *LPSC*, **12B**, 371
- Stadermann, A. C., Zanetti, M. R., Jolliff, B. L., et al. 2018, *Icar*, **309**, 45
- Taylor, G. J., & Martel, L. M. V. 2003, *AdSpR*, **31**, 2403
- Taylor, L. A., & Carrier, W. D., III 1992, *AIAAJ*, **30**, 2858
- Taylor, L. A., & Carrier, W. D., III 1993, in Resources of Near-Earth Space, ed. J. S. Lewis, M. S. Matthews, & M. L. Guerrieri (Tucson, AZ: Univ. Arizona Press), 69
- Thompson, T. W. 1979, *M&P*, **20**, 179
- van der Bogert, C. H., Gaddis, L., Hiesinger, H., et al. 2016, *LPSC*, **47**, 1616
- Vogt, D. S., Schröder, S., Hübers, H.-W., et al. 2020, *LPSC*, **51**, 1385
- Vondrak, R. R., Keller, J., Chin, G., & Garvin, J. 2010, *SSRv*, **150**, 7
- Williams, J.-P., Paige, D. A., Greenhagen, B. T., & Sefton-Nash, E. 2017, *Icar*, **283**, 300
- Wolfe, E. W., Lucchitta, B. K., Reed, V. S., Ulrich, G. E., & Sanchez, A. G. 1975, *LPSC*, **6**, 2463
- Zisk, S. H., Pettengill, G. H., & Catuna, G. W. 1974, *Moon*, **10**, 17